Investigating the Interface of Superhydrophobic Surfaces in Contact with Water

Dhaval A. Doshi,*[,†,⊥] Pratik B. Shah,[‡] Seema Singh,[‡] Eric D. Branson,[‡] Anthony P. Malanoski,[‡,∥] Erik B. Watkins,[†] Jaroslaw Majewski,[†] Frank van Swol,[‡,§] and C. Jeffrey Brinker[‡,§]

Lujan Neutron Scattering Center, Los Alamos National Laboratory, Los Alamos, New Mexico 87545, Center for Micro-Engineered Materials, University of New Mexico, Albuquerque, New Mexico 87106, and Sandia National Laboratories, Albuquerque, New Mexico 87106

Received March 21, 2005. In Final Form: June 11, 2005

Neutron reflectivity (NR) is used to probe the solid, liquid, vapor interface of a porous superhydrophobic (SH) surface submerged in water. A low-temperature, low-pressure technique was used to prepare a rough, highly porous organosilica aerogel-like film. UV/ozone treatments were used to control the surface coverage of hydrophobic organic ligands on the silica framework, allowing the contact angle with water to be continuously varied over the range of 160° (superhydrophobic) to <10° (hydrophilic). NR shows that the superhydrophobic nature of the surface prevents infiltration of water into the porous film. Atomic force microscopy and density functional theory simulations are used in combination to interpret the NR results and help establish the location, width, and nature of the SH film−water interface.

Introduction

We all can recall seeing water droplets "bead up" on the leaves of plants. Most famous is the Lotus leaf, called the "symbol of purity" because of its self-cleaning properties. At very shallow angles of inclination or with the slightest wind, water droplets roll rather than flow.[1,2] The rolling droplets entrain particle contaminants and parasites, thereby cleaning them from the Lotus leaf surface. It is now recognized that the fascinating fluid behaviors observed for the Lotus plant, like the rolling and bouncing of liquid droplets and self-cleaning of particle contaminants, arise from a combination of the low interfacial energy and the rough surface topography of waxy deposits covering their leaves.[3]

Phenomenologically, Cassie and Baxter postulated that the cosine of the contact angle on a heterogeneous solid/air surface is the sum of the cosine of the contact angles of the respective homogeneous surfaces weighted by the surface fraction of the solid,[4,5] $\cos\theta^{*} = -1 + \Phi_s(1 + \cos\theta)$, where θ^{*} is the apparent contact angle, -1 is the cosine of the contact angle of the air surface, and Φ_s is the surface fraction of solid. As the ratio of the pillar width to interpillar distance of a regular lithographically defined surface decreases[6] or the roughness of a random, porous (e.g., fractal) surface increases, Φ_s approaches zero, and θ^{*} approaches 180°. Interestingly, Herminghaus postulates that hierarchical roughness could render any surface (independent of microscopic contact angle) superhydrophobic,[7] but this has not yet been observed. Wenzel had put forward a different relationship for contact angles on rough surfaces:[8] $\cos\theta^{*} = r\cos\theta$, where r is the roughness parameter defined by the ratio of the real surface area to the projected surface area. Because $r \geq 1$, roughness on a hydrophobic surface ($\theta > 90°$) renders it more hydrophobic, whereas on a hydrophilic surface ($\theta < 90°$) roughness has the opposite effect, decreasing θ toward 0°. Although the Wenzel equation is valid when the liquid droplet enters the valleys and completely wets the surface topography, the Cassie−Baxter model requires the presence of a liquid−vapor interface below the droplet.[9] At constant surface roughness, the surface chemistry can be designed to have the contact-angle behavior go from the Wenzel regime to the Cassie−Baxter regime.

Devising synthetic methods to produce superhydrophobic (SH) surfaces is the subject of intensive, ongoing, worldwide research.[10−32] SH properties such as self-

[†] Los Alamos National Laboratory.
[‡] University of New Mexico.
[§] Sandia National Laboratories.
[∥] Currently at the Naval Research Laboratory.
[⊥] Currently at Cabot Corporation, MA 01821.

(1) Barthlott, W.; Neinhuis, C. *Planta (Heidelberg)* **1997**, *202*, 1.
(2) Neinhuis, C.; Barthlott, W. *Ann. Bot. (London)* **1997**, *79*, 667.
(3) Koch, K.; Neinhuis, C.; Ensikat, H. J.; Barthlott, W. *J. Exp. Bot.* **2004**, *55*, 711.
(4) Cassie, A. B. D. *Discuss. Faraday Soc.* **1948**, *3*, 11.
(5) Cassie, A. B. D.; Baxter, S. *Trans. Faraday Soc.* **1944**, *40*, 546.
(6) He, B.; Patankar, N. A.; Lee, J. *Langmuir* **2003**, *19*, 4999.
(7) Herminghaus, S. *Europhys. Lett.* **2000**, *52*, 165.
(8) Wenzel, R. N. *Ind. Eng. Chem.* **1936**, *28*, 988.
(9) Bico, J.; Marzolin, C.; Quere, D. *Europhys. Lett.* **1999**, *47*, 220.
(10) Chen, A. C.; Peng, X. S.; Koczkur, K.; Miller, B. *Chem. Commun.* **2004**, 1964.
(11) Favia, P.; Cicala, G.; Milella, A.; Palumbo, F.; Rossini, R.; d'Agostino, R. *Surf. Coat. Technol.* **2003**, *169/170*, 609.
(12) Feng, L.; Li, S. H.; Li, Y. S.; Li, H. J.; Zhang, L. J.; Zhai, J.; Song, Y. L.; Liu, B. Q.; Jiang, L.; Zhu, D. B. *Adv. Mater.* **2002**, *14*, 1857.
(13) Flemming, M.; Hultaker, A.; Reihs, K.; Duparre, A. *Proc. Soc. Photo-Opt. Instrum. Eng.* **2003**, *5250*, 56.
(14) Khorasani, M. T.; Mirzadeh, H.; Sammes, P. G. *Radiat. Phys. Chem.* **1996**, *47*, 881.
(15) Klein, R. J.; Biesheuvel, R. M.; Yu, B. C.; Meinhart, C. D.; Lange, F. F. *Z. Metallkd.* **2003**, *94*, 377.
(16) Nakajima, A.; Abe, K.; Hashimoto, K.; Watanabe, T. *Thin Solid Films* **2000**, *376*, 140.
(17) Ren, S. L.; Yang, S. R.; Zhao, Y. *Acta Mech. Sinica* **2004**, *20*, 159.
(18) Sasaki, M.; Kieda, N.; Katayama, K.; Takeda, K.; Nakajima, A. *J. Mater. Sci.* **2004**, *39*, 3717.
(19) Shirtcliffe, N. J.; Sanaa, A.; Evans, C.; McHale, G.; Newton, M. I.; Perry, C. C.; Roach, P. *J. Micromech. Microeng.* **2004**, *14*, 1384.
(20) Teare, D. O. H.; Spanos, C. G.; Ridley, P.; Kinmond, E. J.; Roucoules, V.; Badyal, J. P. S.; Brewer, S. A.; Coulson, S.; Willis, C. *Chem. Mater.* **2002**, *14*, 4566.
(21) Woodward, I.; Schofield, W. C. E.; Roucoules, V.; Badyal, J. P. S. *Langmuir* **2003**, *19*, 3432.
(22) Feng, L.; Li, S. H.; Li, H. J.; Zhai, J.; Song, Y. L.; Jiang, L.; Zhu, D. B. *Angew. Chem., Int. Ed.* **2002**, *41*, 1221.
(23) Zhang, X.; Shi, F.; Yu, X.; Liu, H.; Fu, Y.; Wang, Z. Q.; Jiang, L.; Li, X. Y. *J. Am. Chem. Soc.* **2004**, *126*), 3064.
(24) Shin, J. Y.; Kuo, C. W.; Chen, P. L.; Mon, C. Y. *Mater. Res. Soc. Symp. Proc.* **2004**, *823*, 181.
(25) Shirtcliffe, N. J.; McHale, G.; Newton, M. I.; Chabrol, G.; Perry, C. C. *Adv. Mater.* **2004**, *16*, 1929.

10.1021/la050750s CCC: $30.25
Published on Web 07/23/2005

cleaning, water exclusion, avoidance of corrosion, and promotion of slip suggest numerous applications from protective coatings, MEMS, and aerosol collection to new protective fabrics for military use.[33,34] The nature of the water/SH surface is crucial to the realization of these practical applications. Of particular interest is understanding how this solid−liquid−vapor interface controls phenomena such as rolling[35] instead of sliding of individual droplets and avoiding the nearly ubiquitous no-slip boundary condition.[36−41]

We have developed a simple, evaporation-driven procedure to deposit fractal SH coatings on arbitrary surfaces. It is derived from our earlier work on low-temperature/low-pressure aerogel coatings.[42] In this process, surface derivatization of silica sols with fluroalkyl groups[28] causes drying shrinkage to be reversible. Springback at the final stage of drying results in a hierarchical fractal surface decorated with hydrophobic ligands. The advantage of our approach relative to many others is that SH surfaces form by (evaporation-induced) reassembly from a very low viscosity sol under standard laboratory conditions. This makes our procedure amenable to coating small features and virtually any kind of substrate. Applied to plastic, glass, metal, and silicon substrates and textiles, our SH coatings are optically transparent with contact angles exceeding 155°. In addition, we have developed a lithographic technique enabling optical adjustment of the water contact angle from 170° to <10°.

SH fractal surfaces with surface fractal dimension of 2.2−2.3 have also been formed by freezing an alkylketene dimer wax[31,43] or by surface treatment of anodically oxidized alumina films with fluoroalkyl ligands,[32,44] whereas for our SH aerogel films a mass fractal dimension of 2.7 is measured using small-angle X-ray scattering.

Although scanning electron microscopy (SEM) and atomic force microscopy (AFM) have been used routinely to image SH surfaces in air, a noninvasive technique such as X-ray or neutron scattering is required to study the buried water−SH film interface. Neutrons are particularly useful for such a study because of their large penetration depth, isotopic sensitivity, and ability to contrast match portions of the system. Neutron reflectivity (NR) has been used to study buried thin films and their interfaces;[45−47] it provides information about the scattering-length density, thickness, and interfacial roughness of different layers in a system.

Here, neutron reflectivity is used to understand the properties of superhydrophobic films in contact with water. UV/ozone treatment is used to vary the water contact angle and understand the resulting effect on the SH film interaction with deuterated water (D_2O). Comparing AFM results, DFT simulations, and NR, we arrive at the location, width, and nature of the SH−water interface.

Experimental Methods

SH Film Preparation. The superhydrophobic coatings were made from a precursor solution containing mixed alkoxides 3,3,3-trifluoropropyl-trimethoxysilane (TFPTMOS) and tetramethyl orthosilicate (TMOS) using a variation of the aerogel thin film process reported by Prakash et al.[42] The filtered sol was further diluted with ethanol and other solvents to obtain a final film thickness of ∼50 nm. Water contact angles consistently reached 155−160°, and angles up to 170° have been observed. The advancing and receding contact-angle hysteresis is typically 5°. The effect of various process parameters on the superhydrophobic behavior of the aerogel films is the topic of another communication.

To prevent the potential dissolution of underivatized silica in the aqueous subphase[48,49] during the long acquisition times of NR (approximately 4 h), the D_2O subphase used in this study was made acidic by adding D_2SO_4 so as to make the final acid concentration 0.01 N (approximately equivalent to pH 2). No treatment to remove dissolved gases from D_2O was performed. To investigate the SH−water interface further, contrast matching experiments were performed with an acidic water subphase composed of a mixture of H_2O and D_2O (referred to as HDO henceforth) in the v/v ratio of 17:4, resulting in a water subphase scattering-length density (SLD) of 0.75×10^{-6} Å^{-2}. Contrast matching techniques allow certain regions of the film to be enhanced or diminished with respect to neutron scattering.

UV/ozone treatment was performed to photocalcine the organic ligands.[50,51] The time of exposure controlled the surface occupancy of the CH_3 and CF_3 groups, thereby adjusting the apparent contact angle, θ^{α}, while maintaining constant porosity, Φ_s, and roughness

AFM/SEM/TEM. Various microscopies were used to investigate the surface and bulk structure of the SH films. Scanning electron microscopy (SEM) was performed on a Hitachi S-800, equipped with a Gatan CCD (charged coupled device) camera at an operating voltage of 20 kV. Samples were coated with a thin gold film to prevent charging. Transmission electron microscopy (TEM) measurements were performed on a JEOL 2010 microscope to investigate the internal fractal structure of the aerogel film. Film fragments were scraped from the substrate and transferred onto a holey carbon grid for investigation. Atomic force microscopy (AFM) measurements were performed on a Digital Instruments Nanoscope IIIa SPM controller (noise < 0.3 Å rms in the vertical, i.e., z , dimension, with vibration isolation) in contact mode. A cantilever with a nominal spring constant of 0.1 N/m was used with minimum force (the tip was withdrawn stepwise and brought back stepwise to track the surface). The images are 512 pixels × 512 pixels in size, hence the scan size determined the resolution.

DFT Simulations. To investigate the contact region of a fluid and a rough substrate, we performed lattice modeling. On a 3D lattice, we constructed a wall with a regular array of square pyramids. The wall sites that make up the pyramids interact with the fluid via a short-ranged one-body external field whose strength is such that a smooth wall of these sites would have a contact angle somewhat larger than 90°. The fluid in question

(26) Kijlstra, J.; Reihs, K.; Klamt, A. *Colloids Surf., A* **2002**, *206*, 521.
(27) Brevnov, D. A.; Barela, M. J.; Brooks, M. J.; Lopez, G. P.; Atanassov, P. B. *J. Electrochem. Soc.* **2004**, *151*, B484.
(28) Roig, A.; Molins, E.; Rodriguez, E.; Martinez, S.; Moreno-Manas, M.; Vallribera, A. *Chem. Commun.* **2004**, 2316.
(29) Shang, H. M.; Wang, Y.; Limmer, S. J.; Chou, T. P.; Takahashi, K.; Cao, G. Z. *Thin Solid Films* **2005**, *472*, 37.
(30) Rao, A. V.; Kulkarni, M. M.; Amalnerkar, D. P.; Seth, T. *J. Non-Cryst. Solids* **2003**, *330*, 187.
(31) Onda, T.; Shibuichi, S.; Satoh, N.; Tsujii, K. *Langmuir* **1996**, *12*, 2125.
(32) Shibuichi, S.; Yamamoto, T.; Onda, T.; Tsujii, K. *J. Colloid Interface Sci.* **1998**, *208*, 287.
(33) Inoue, Y. *J. Jpn Soc. Tribol.* **2002**, *47*, 353.
(34) Blossey, R. *Nat. Mater.* **2003**, *2*, 301.
(35) Richard, D.; Quere, D. *Europhys. Lett.* **1999**, *48*, 286.
(36) Barrat, J. L.; Bocquet, L. *Phys. Rev. Lett.* **1999**, *82*, 4671.
(37) Baudry, J.; Charlaix, E.; Tonck, A.; Mazuyer, D. *Langmuir* **2001**, *17*, 5232.
(38) Tretheway, D. C.; Meinhart, C. D. *Phys. Fluids* **2002**, *14*, L9.
(39) Zhu, Y. X.; Granick, S. *Phys. Rev. Lett.* **2002**, *88*, 106102.
(40) Granick, S.; Zhu, Y. X.; Lee, H. *Nat. Mater.* **2003**, *2*, 221.
(41) Ou, J.; Perot, B.; Rothstein, J. P. *Phys. Fluids* **2004**, *16*, 4635.
(42) Prakash, S. S.; Brinker, C. J.; Hurd, A. J.; Rao, S. M. *Nature* **1995**, *374*, 439.
(43) Shibuichi, S.; Onda, T.; Satoh, N.; Tsujii, K. *J. Phys. Chem.* **1996**, *100*, 19512.
(44) Tsujii, K.; Yamamoto, T.; Onda, T.; Shibuichi, S. *Angew. Chem., Int. Ed. Engl.* **1997**, *36*, 1011.
(45) Fragneto-Cusani, G. *J. Phys.: Condens. Matter* **2001**, *13*, 4973.
(46) Krueger, S. *Curr. Opin. Colloid Interface Sci.* **2001**, *6*, 111.
(47) Wu, W. L.; Orts, W. J.; Majkrzak, C. J.; Hunston, D. L. *Poly. Eng. Sci.* **1995**, *35*, 1000.
(48) Iler, R. K. *The Chemistry of Silica*; Wiley: New York, 1979″.
(49) Brinker, C. J.; Scherer, G. W. *Sol−Gel Science: The Physics and Chemistry of Sol−Gel Processing*; Academic Press: San Diego, CA, 1990.
(50) Clark, T.; Ruiz, J. D.; Fan, H. Y.; Brinker, C. J.; Swanson, B. I.; Parikh, A. N. *Chem. Mater.* **2000**, *12*, 3879.
(51) Dattelbaum, A. M.; Amweg, M. L.; Ruiz, J. D.; Ecke, L. E.; Shreve, A. P.; Parikh, A. N. *Mater. Res. Soc. Symp. Proc.* **2003**, *788*, 371.

is a lattice gas model fluid with short-range attractions that reach to the next nearest neighbor sites. The temperature is about halfway between the triple and critical points, and together with the choice of overall density, this ensures that two-phase coexistence will be maintained. We used lattice density functional theory (DFT) in the canonical ensemble to minimize the total Helmholtz free energy and solve for the equilibrium density profile.[52,53] The initial configuration consisted of an isolated drop in the middle of the box. The drop can then be lowered, for instance, by applying a slight gravitational field. Ultimately, the drop enters the interaction range of the patterned wall, and the drop adjusts its shape to minimize the surface free energy.

Neutron Reflectivity. The reflectivity R of a surface is defined as the ratio of the number of particles (neutrons or photons) elastically and specularly scattered from the surface to the number of incident particles. When measured as a function of wave vector transfer, Q_z (defined below), the reflectivity curve contains information regarding the profile of the in-plane average of the coherent scattering cross sections normal to the substrate (silicon surface). If one knows the chemical constituents of the investigated system and the concentration of a given atomic species at a particular depth, z, then the scattering length density (SLD) distribution, $\beta(z)$, can be calculated from

$$\beta(z) = \frac{1}{v_m(z)}\sum_i^m b_i(z)$$

where b_i is the bound coherent scattering length of the ith of m atoms in the molecule with molecular volume v_m at location z. In the first Born approximation, the specular reflectivity, R, is related to the Fourier transform of the spatial derivative of the scattering-length density profile, $d\beta/dz$, by

$$R(Q_z) = R_F(Q_z)\left|\frac{1}{\beta_s}\int_{-\infty}^{+\infty}\frac{d\beta(z)}{dz}\exp(-iQ_z z)\,dz\right|^2$$

where R_F is the Fresnel reflectivity of the substrate and β_s is the substrate scattering-length density. Neutron reflectivity measurements were performed on the SPEAR beamline, a time-of-flight reflectometer, at the Manuel Lujan Neutron Scattering Center, Los Alamos National Laboratory (http://lansce.lanl.gov/lujan/index_lujan.htm). The neutron beam is produced by the spallation of neutrons from a tungsten target using a pulsed beam (20 Hz) of 800 MeV protons. A partially coupled liquid-hydrogen moderator at 20 K modifies the neutron energy spectrum. Neutrons with wavelengths of $\lambda = 2-16$ Å are selected by means of choppers and frame-overlap mirrors (http://www.lansce.lanl.gov/lujan/ER1ER2/SPEAR/index.html). The scalar value of momentum transfer vector Q_z is determined from $Q_z = 4\pi\sin(\alpha)/\lambda$ (where α is the angle of incidence measured from the sample surface and λ is the wavelength of the probe), and its range is covered by performing measurements at two angles of incidence, typically 0.5 and 2.5°. The beam footprint was 8 mm × 60 mm. The background limits the Q_z range over which reflectivity data can be collected; scattering from the subphase makes a significant contribution to the background. Hence, we designed a cell made of Maycor (Ceramic Products Inc, Palisades Park, NJ, containing $SiO_2/MgO/Al_2O_3/K_2O/B_2O_3/F$ in the weight ratio 46:17:16:10:7:4) to minimize the incoherent scattering from the cell, and the O-ring groove was machined to achieve a subphase reservoir depth of about 50 μm (Figure 1).

The reflectivity data is normalized by the Fresnel reflectivity of the substrate, R_F, and plotted versus Q_z to compensate for the sharp decrease in the reflectivity[54] as described by Fresnel's law: $R \propto Q_z^{-4}$.

The intensity of the specular reflectivity and the real-space SLD are related by a transformation. Because phase information is lost when collecting the specular reflectivity, as in most scattering experiments, and because of the nonlinear nature of the inverse transformation, a unique solution to the problem cannot be obtained analytically. The reflectivity data were analyzed by a model-dependent Parratt formalism[55] that requires a priori knowledge of the composition of the sample (SLD profile). Here our philosophy was to use the simplest possible model of physical relevance. In this model, the scattering-length density distribution $\beta(z)$ is described by a sequence of n slabs, each of constant scattering-length density. Two adjoining layers i and $i+1$ are connected by β_{int}, a sigmoidal function profile that describes the interfacial (chemical) roughness given by

$$\beta_{int}(z) \propto \mathrm{erf}\left(\frac{z - z_{mid}}{\sigma}\right)$$

The error function is symmetric around z_{mid}, and so is the resulting interface profile. This is used as a convenient, well-accepted model. We recognize that interfaces may not be symmetric, but because of the lack of a priori information from other experiments and theory, we are limited to the use of symmetric profiles to reduce the number of parameters in the fit and arrive at the simplest possible model.

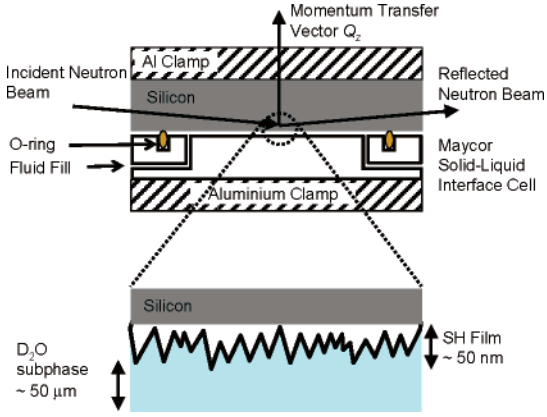

Figure 1. Schematic of the setup used for neutron reflectivity measurements.

Results and Discussion

Surface Characterization. Superhydrophobic (SH) films were spin coated onto 10-cm-diameter, 6-mm-thick silicon substrates. Spectroscopic ellipsometry measurements indicate a film thickness of 440 Å and a refractive index of $n_f = 1.1188$. Assuming an all-silica skeleton (X-ray photon spectroscopy measurements indicate low amounts of organics (C, H, F)), the z-averaged film porosity can be determined from the Lorenz−Lorentz relationship[49]

$$\frac{n_f^2 - 1}{n_f^2 + 2} = (1 - \phi)\frac{n_s^2 - 1}{n_s^2 + 2}$$

where n_s is the refractive index of the solid skeleton and ϕ is the film porosity. Using the above equation and $n_s = 1.458$, we obtain a porosity value of $\phi = 0.72$. (This value represents a lower bound for the porosity due to the presence of C, F, and H.) Sessile drop contact-angle measurements on SH films indicate an apparent water contact angle of 158 ± 2° (Figure 2).

Panels A and B of Figure 3 show SEM micrographs of the film surface. The lighter regions correspond to silica, whereas the dark regions represent pores in the network. The globular morphology typical of a base-catalyzed silica gel is seen. The broad distribution of globular building blocks that results in the rough surface and imparts to the film its superhydrophobic character is evident from these images. The TEM image in Figure 4 shows the

(52) Van Swol, F.; Malanoski, A. P. *Phys. Rev. E: Stat. Phys., Plasmas, Fluids, Relat. Interdiscip. Top.* **2002**, *66*, 041603/1.
(53) Van Swol, F.; Malanoski, A. P. *Phys. Rev. E: Stat. Phys., Plasmas, Fluids, Relat. Interdiscip. Top.* **2002**, *66*, 041602/1.
(54) Als-Nielsen, J. *Physica A* **1986**, *140*, 376.
(55) Parratt, L. *Phys. Rev.* **1954**, *95*, 359.

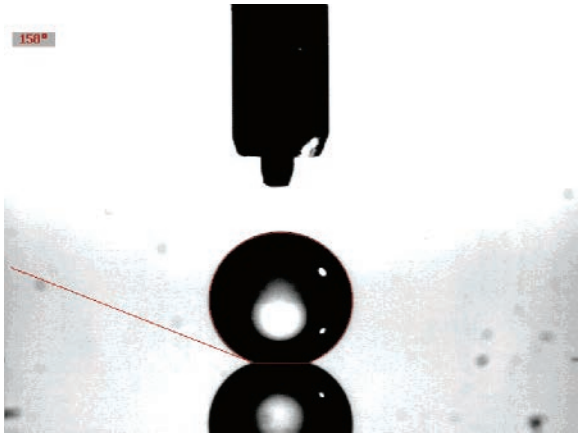

Figure 2. Representative image of a sessile drop measurement of the water contact angle on a superhydrophobic aerogel film showing a contact angle of 158 ± 2°.

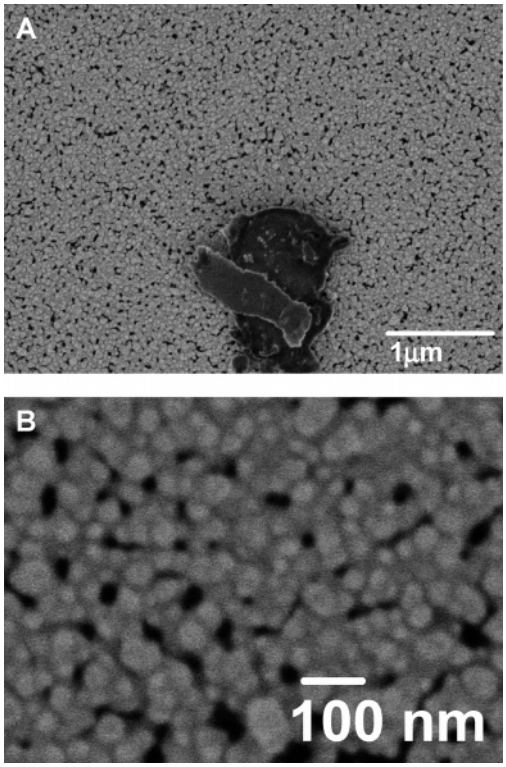

Figure 3. Scanning electron micrographs of the SH Film. (A) Top view of the SH film. The dust particle at the bottom center is used as a focusing aid. (B) Higher-magnification image of the same film. The slight rounding of the features is due to the gold coating. The lighter regions correspond to silica, whereas the dark regions represent pores in the network.

porous nature of the film. The darker regions correspond to silica, whereas the lighter regions represent the porous network. This open-cell structure exhibits fractal porosity with a wide pore-size distribution ranging from 1 to 500 nm.[56] Figure 5 shows a contact-mode AFM image of the rough SH film in air. The calculated rms roughness, measured over the area 13.5 μm × 13.5 μm, is $\sigma_{AFM} = 123$ Å. The inset in Figure 5 shows a higher-resolution AFM image with a 1.5 μm × 1.5 μm scan size. The inset shows the presence of roughness at various length scales, and the calculated rms roughness is 11 Å. Because the coherence of the incident neutron beam in the neutron

(56) Prakash, S. S.; Brinker, C. J.; Hurd, A. J. *J. Non-Cryst. Solids* **1995**, *190*, 264.

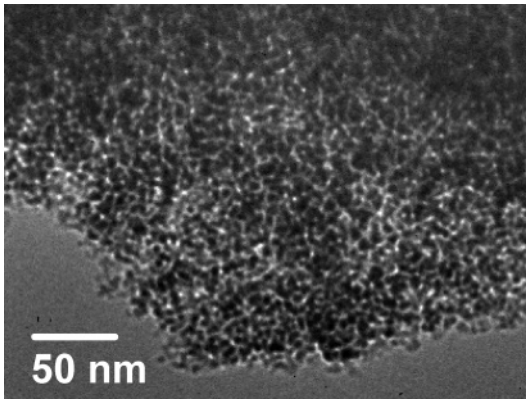

Figure 4. Transmission electron micrograph of the superhydrophobic aerogel film. The darker regions correspond to silica, whereas the lighter regions represent the porous network.

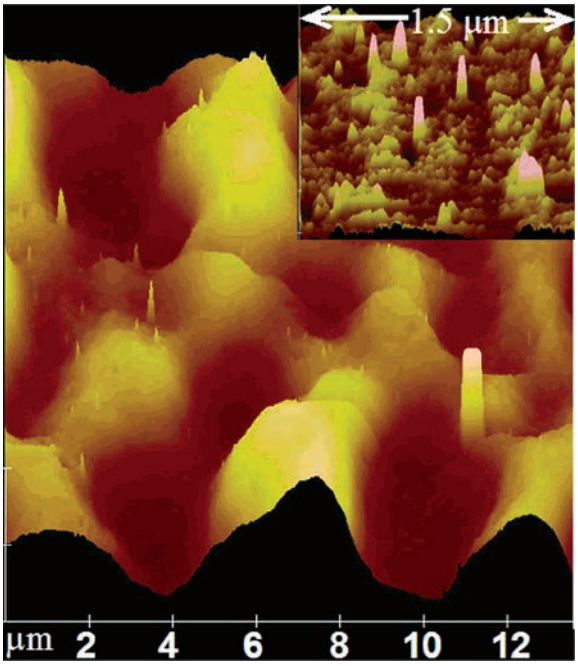

Figure 5. AFM image of SH film in air measured over an area of 13.5 μm × 13.5 μm. The inset shows another image at a higher magnification measured over an area of 1.5 μm × 1.5 μm.

reflectivity measurements is approximately 10 μm, for a comparison of roughness with neutron reflectivity data the larger scan size image in Figure 5 is relevant.

Neutron Reflectivity. Figure 6A shows the normalized reflectivity data for superhydrophobic aerogel films in contact with two different aqueous environments. The use of 100% D_2O and a H_2O/D_2O mixture (referred to as HDO) allows us to study the system using two different scattering contrasts. The corresponding SLD profiles are shown in Figure 6B. It is evident from the SLD profile, especially in the case of a 100% D_2O subphase, that the porous SH film experiences minimal water penetration into the film bulk. Assuming no water penetration and a pure silica matrix with an SLD value of 3.47×10^{-6} Å^{-2} (neglecting the contribution from the CH_3 and CF_3 groups), we find that an SLD value of $(0.353 \pm 0.12) \times 10^{-6}$ Å^{-2} for the SH film (see region 20 Å < z < 200 Å in Figure 6B) corresponds to a porosity of $\{(1 - (0.353/3.47)\} \times 100 = 90 \pm 3\%$, which is consistent with nitrogen adsorption measurements.[42,56] The film thickness obtained from the fit, $t = 425 \pm 6$ Å, is consistent with ellipsometry data. The fitted value of the roughness of the SH film−water

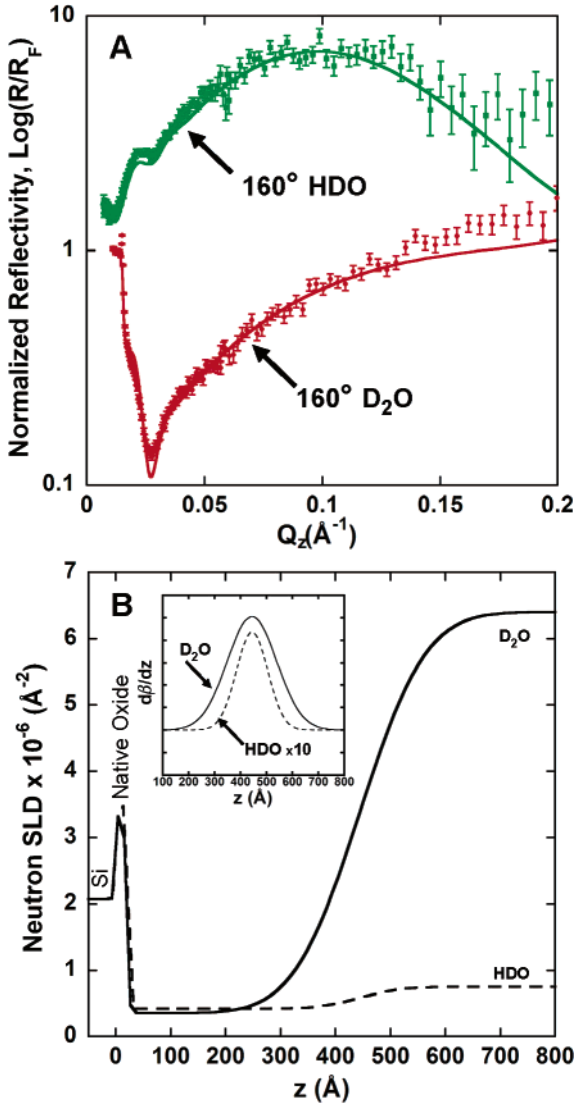

Figure 6. (A) Fresnel normalized reflectivity data and fit for a superhydrophobic film with a water contact angle of 160° in contact with 100% D_2O and a D_2O-H_2O mixture (labeled HDO). (B) Corresponding SLD profile for the fits in A. (Inset in B) Derivative of the SLD profiles in B, showing the location and width of SH film−water interface.

interface using an error function profile, $\mathrm{erf}\{(z - z_{mid})/\sigma\}$, is $\sigma_{SH-D_2O} = 95 \pm 3$ Å. This value is comparable to the rms roughness determined from AFM experiments.

As mentioned earlier, studying the same system against a different subphase contrast provides additional information about the system and also corroborates the values of the fit parameters. For the SH film measured against a H_2O/D_2O mixture (HDO), the SLD of the bulk SH film described by the region with uniform SLD (20 Å $< z <$ 200 Å in Figure 6B) is comparable to the case when the subphase is 100% D_2O. The fitted thickness of the SH film, 422 ± 10 Å, is again similar to the previous case. The inset in Figure 6B shows the derivative of the SLD profile, $d\beta/dz$, where the lower full width of the Gaussian (the derivative of an error function is a Gaussian) in the case of the HDO indicates a smaller interfacial roughness of $\sigma_{SH-HDO} = 60 \pm 4$ Å This apparent reduction in roughness can be attributed to the lower SLD contrast between the SH film and bulk water, where certain valleys in the surface topography that may be filled with the water subphase cannot be discerned from the bulk water or the bulk film.

The difference in the SLD as one approaches bulk water can be written as

$$\Delta\beta = \beta_{film}\epsilon_{film} + \beta_{water}(1 - \epsilon_{film}) - \beta_{water}$$
$$= (\beta_{film} - \beta_{water})\epsilon_{film}$$

where ϵ_{film} is the areal fraction occupied by the film at a particular z value, $\beta_{film} = 0.35 \times 10^{-6}$ Å^{-2}, $\beta_{D_2O} \approx 6.3 \times 10^{-6}$ Å^{-2}, and $\beta_{H_2O/D_2O} = 0.75 \times 10^{-6}$ Å^{-2}. Given a constant $\Delta\beta$ resolving ability of NR, the apparent bulk water will be detected at a lower ϵ_{film} value for the mixed H_2O/D_2O subphase, which corresponds to a smaller z value. A reduction of approximately 100 Å in the z location of bulk water (seen clearly by the tail of the Gaussian peak in the $d\beta/dz$ profile in the Figure 6B inset) for the mixed H_2O/D_2O subphase suggests that water penetrates to a depth of at least 100 Å from the thickest location of the SH film.

The neutron reflectivity (NR) data also helps us eliminate certain possibilities that one might envisage for the nature of the water−film interface. We have considered alternative scenarios; one probable one is where a flat, smooth water surface spans the peaks of the surface roughness without entering the valleys. A model constrained to include a rough film surface but with a smooth water surface cannot fit the NR data. This information along with the fact that different subphase contrast experiments (D_2O and HDO subphase) show different roughness suggests that the real situation is akin to an Indian fakir on a bed of nails with his skin sagging between the nails.

The proposed situation is described by the DFT simulations in Figure 7, where we display the final 3D contour-level density profile of the drop as it has come to rest on the pyramids. The results demonstrate that whereas the local contact angle (where fluid and pyramids meet locally) is indeed slightly larger than 90° the overall effective contact angle is close to 180°. The limited contact points between the liquid droplet and the solid surface as seen from Figure 7B may aid the rolling motion of the droplet as seen for the lotus leaf, as opposed to sliding.

Figure 8A shows normalized neutron reflectivity data and fits for aerogel films with water contact angles of <10, 100, or 160° in contact with D_2O. The corresponding SLD profile derived from box model fits is shown in Figure 8B. It is evident from the SLD profiles that the superhydrophobic film with a contact angle of 160° shows minimal water infiltration, as evident by the low SLD values next to the silicon substrate (same data as in Figure 6).

In the case of a film subjected to 30 min of photocalcination to remove the hydrophobic groups and render it hydrophilic (water contact angle of <10°) but maintain its surface topography (roughness), we do observe D_2O infiltration into the porous aerogel matrix. The SLD of the D_2O filled film (region 100 Å $< z <$ 220 Å in Figure 8B) is $(5.87 \pm 0.04) \times 10^{-6}$ Å^{-2}, and that of the bulk D_2O subphase ($z >$ 600 Å) is 6.27×10^{-6} Å^{-2}. These values indicate a D_2O volume occupancy of $(5.87 - 0.353)/6.27 \times 100 = 87 \pm 3\%$ in the aerogel film, which, considering complete infiltration into open pores, is consistent with the earlier deduced porosity of 90 ± 3%. The small difference can be attributed to 3.3% closed and/or inaccessible pores. Furthermore, the location of the average film−D_2O interface, marked by the inflection point in the SLD profile or, alternatively and more clearly, the position of the Gaussian peak (Figure 8C) in the derivative of the SLD profile is preserved for both the <10 and 160° contact-angle samples. The fitted roughness value is $\sigma_{10deg-D_2O} = 86 \pm 20$ Å.

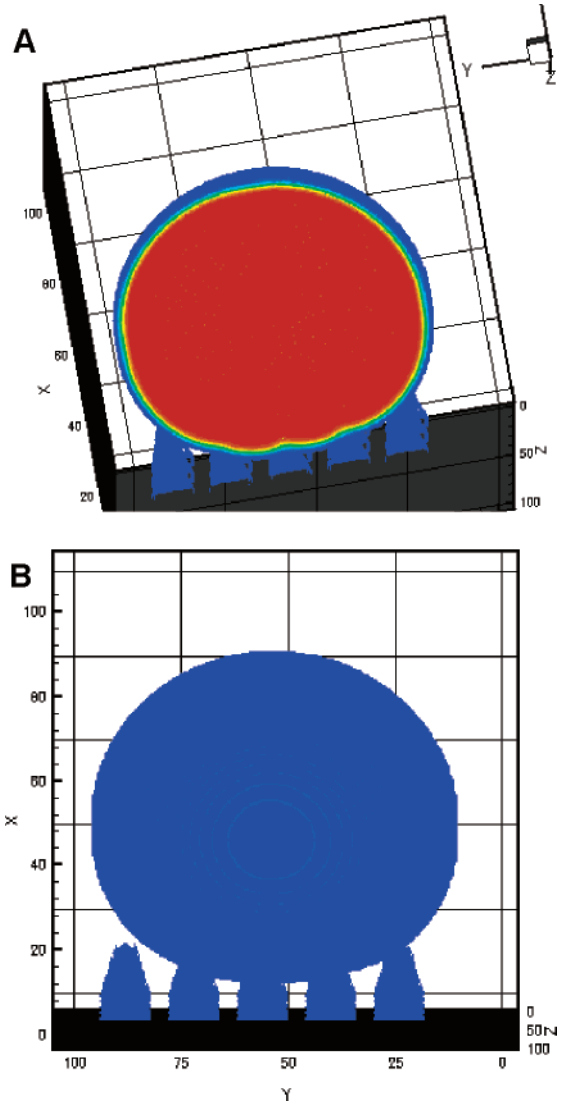

Figure 7. DFT simulation of a 40 nm water droplet on a rough surface: (A) a top-angled view and (B) a side cross-sectional view.

For an SH film subjected to partial photocalcination such that its surface exhibits a water contact angle of 100°, we observe behavior that is intermediate between that of the 160 and <10° contact-angle samples. From the normalized reflectivity curve in Figure 8A, we see that the intensity increases toward unity with decreasing contact angle. That is, the difference between the sample reflectivity, R, and the Fresnel reflectivity, R_F, decreases, indicating a reduction in the contrast between the bulk and the porous film (due to filling of the pores with D_2O). The SLD profile for the 100° film indicates the existence of a continuous gradient from bulk D_2O into the film. This gradient can be attributed to the distribution of pockets of pores that are not filled by water. Pores with a surface contact angle greater than 90° should not get filled with water. Because the film surface contact angle is amplified by its roughness,[5,8] the corresponding contact angle for identical surface chemistry that exists within the pores may be less than 90°. This allows water to infiltrate pores of size greater than a certain critical size, resulting in a distribution of water-filled and empty (air-filled) pores. This distribution results in a chemical roughness (roughness in SLD) to which the neutrons are sensitive. The peak in the SLD derivative profile seen around 300 Å (Figure 8C) does not imply that the average film thickness has been reduced to 300 Å. Instead, it is a manifestation of the chemical roughness. There is consistency in the

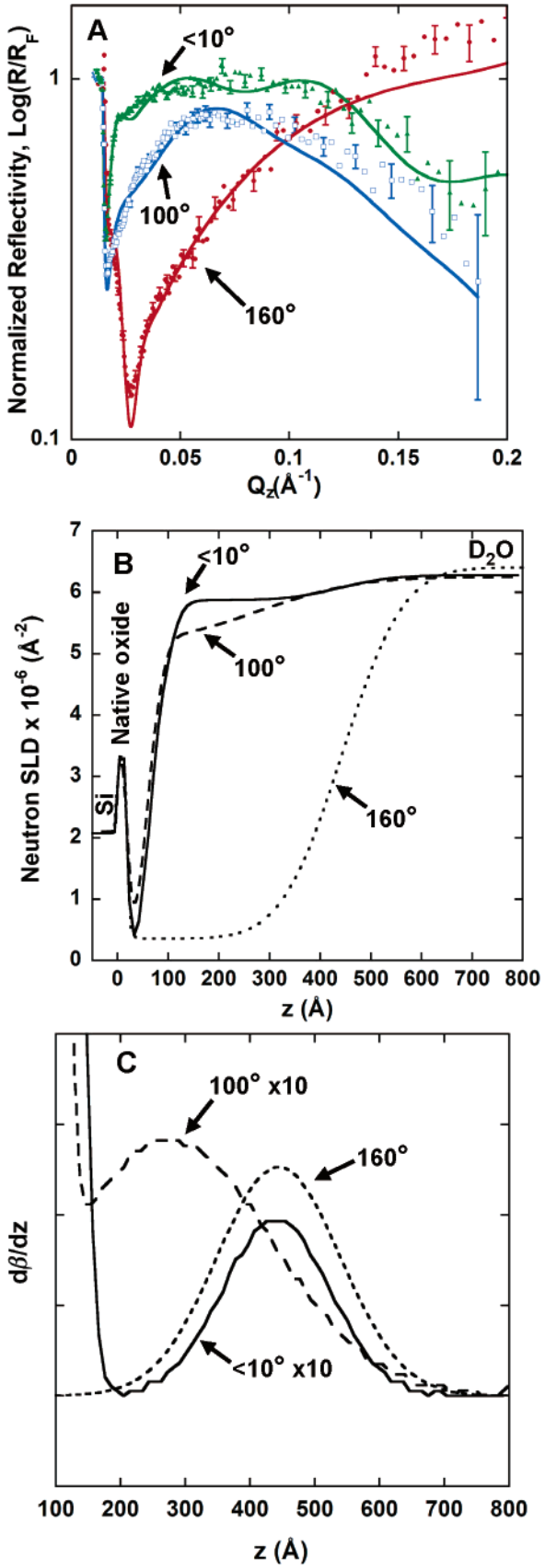

Figure 8. (A) Fresnel normalized reflectivity data and fit for films with different contact angles in contact with D_2O. (B) Corresponding SLD profile for the fits in A. (C) Derivative of the SLD profiles in B, showing the location and width of interfaces in the system.

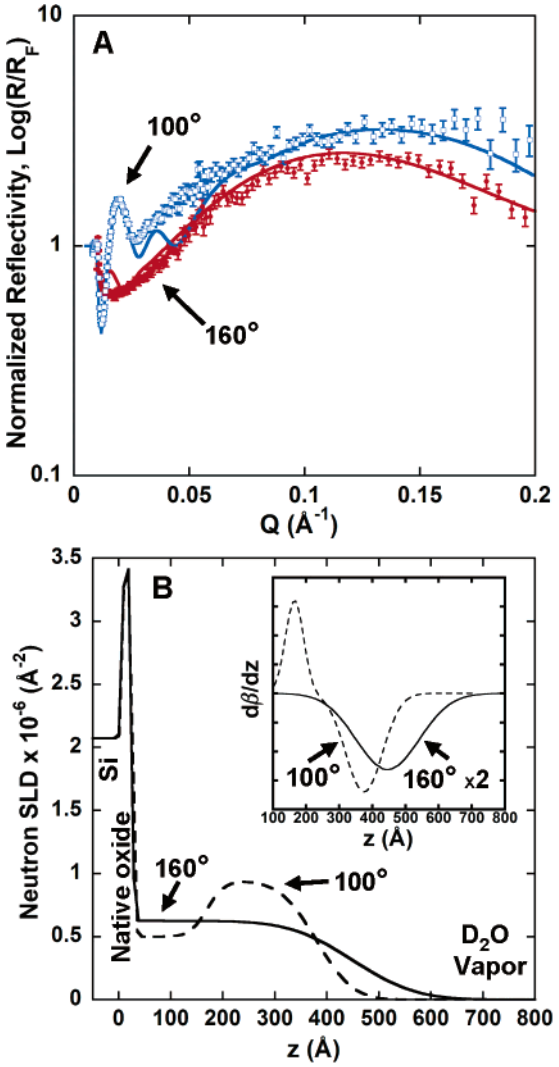

Figure 9. (A) Fresnel normalized reflectivity data and fit for films with different contact angles in contact with D_2O vapor. (B) Corresponding SLD profile for the fits in A. (Inset in B) Derivative of the SLD profiles in B, showing the location and width of interfaces in the system.

three contact-angle films studied regarding the z location of bulk D_2O that is found at about 600 Å.

A feature that is common to the <10 and 100° contact-angle films and might also be present in the 160° contact-angle film is the presence of a buried layer of 33−37 Å thickness at the substrate film interface (20 Å < z < 60 Å) that exhibits almost no D_2O penetration. Its presence and length scale can also be seen from the normalized reflectivity curves that show a broad but definite envelope with an approximate width of $\Delta Q_z = {}^{2\pi}/_{37} = 0.16$ Å^{-1}, a feature that is clearly absent in the 160° SH film data. The presence of this layer can be explained by either (i) trapped and stabilized gas bubble pockets during cell filling or (ii) a different film morphology that forms during the coating or the photocalcination process next to the solid substrate compared to the bulk and gives rise to a more closed-cell structure preventing water penetration.

Figure 9 shows the normalized neutron reflectivity and SLD profiles for films with contact angles of 160 and 100° exposed to a saturated D_2O vapor environment. The lack of scattering contrast between the SH film (160°) and the D_2O vapor, coupled with a high surface roughness, results in an almost featureless reflectivity curve. Hence, the SH film thickness and interfacial roughness parameter σ were fixed, on the basis of values obtained previously against a D_2O subphase, at 425 and 95 Å, respectively. A bulk film SLD of 0.62×10^{-6} Å^{-2} was obtained. The increase in the SLD value from that of a 90% porous silica may be due to D_2O condensation into defects and/or the constrained fit. However, this provides a baseline to compare qualitatively with a film prepared with a surface water contact angle of 100° shown in Figure 9. The reflectivity curve for the 100° film shows a clear oscillation in the Q_z range of 0.01−0.03 Å^{-1}. This oscillation most likely arises from a layer of higher SLD contrast and/or greater smoothness. The SLD profile for this film shows evidence of water condensation into the pores of the film. The region 120 Å < z < 300 Å in Figure 9B exhibits an SLD of $(0.94 \pm 0.05) \times 10^{-6}$ Å^{-2} indicating approximately 10% of the pore space to be filled with condensed D_2O. A smoother interface is also seen as a narrower peak width in the derivative profile in the inset of Figure 9B. This maybe attributed to a skin of water-filled pores forming at the film surface reducing the effective chemical (SLD) roughness seen by neutrons.

Conclusions

NR combined with additional structural analyses and molecular simulations has established the nature of rough silica surfaces submerged in water or exposed to 100% RH. For SH surfaces characterized by water contact angles of ~160°, water penetrates to a depth of about 100 Å, which is on the order of the surface roughness probed by AFM. At this level of penetration, the interface comprises about 5% solid, and the interface is defined by the topology of the pinned solid/liquid/vapor contact points. Using 5% solid and 91° for θ, we derive an apparent contact angle, θ^{∞}, of 154° from the Cassie−Baxter relationship. The complete removal of hydrophobic ligands via photocalcination (θ < 10°), while preserving the roughness, should yield θ^{∞} > 130° according to the Cassie−Baxter relationship. However, this is not observed, which suggests that we are in the Wenzel regime. The inherent presence of air in the porous aerogel films may be a contributing factor to the validity of the Cassie−Baxter regime, but when the hydrophobic ligands are removed, the Wenzel regime is thermodynamically favorable. This mix of trapped air and surface roughness makes these films an interesting system to study from a theoretical viewpoint. Observing such a high water contact angle for a film of <500 Å thickness is remarkable when compared to the micrometer-scale roughness developed in most synthetic SH surfaces and found in nature.[2,3] Photocalination procedures allow a change in surface chemistry with minimal effect on surface topography. A systematic trend of increased water infiltration with decreasing surface coverage of the hydrophobic ligands is observed. Surprisingly, an ~35 Å buried layer with low scattering-length density is observed in photocalcined films. Its origin is not well understood and will be the subject of future investigations.

Acknowledgment. We thank Dr. W. Hamilton (ORNL) for the use of the MIRROR fitting program and Dr. C. Braun (HMI-Berlin, Germany) for the Parratt32 reflectivity program. D.A.D. acknowledges support from the LANL Director's Postdoctoral Fellowship. This work was supported by Los Alamos National Laboratory under DOE contract W7405-ENG-36, the DOE Office of Basic Energy Science, Sandia National Laboratories' Lab-Directed Research and Development program, the Air Force Office of Scientific Research, and the Army Research Office.

LA050750S